IEEE Access
Multidisciplinary | Rapid Review | Open Access Journal

Received November 25, 2018, accepted December 28, 2018, date of publication February 1, 2019, date of current version February 12, 2019.

Digital Object Identifier 10.1109/ACCESS.2019.2891165

Design and Analysis of Triplen Controlled Resonant Converter for Renewable Sources to Interface DC Micro Grid

SNEHAL PACHPOR[1] AND HIRALAL MURLIDHAR SURYAWANSHI[2,3], (Senior Member, IEEE)
[1]Department of Electrical Engineering, Kavikulguru Institute of Technology and Science, Ramtek 441106, India
[2]Department of Electrical Engineering, Visvesvaraya National Institute of Technology 440010, Nagpur, India
[3]Department of Electrical Engineering, Indian National Academy of Engineering, New Delhi 110016, India

Corresponding author: Snehal Pachpor (pachporsnehal2@gmail.com)

ABSTRACT This paper presents a triplen controller for a dc–dc resonant converter, which provides excellent load voltage regulation with respect to wide variations in input voltage from renewable sources in a dc micro grid. The control provides enhanced converter efficiency and soft switching of all the switches from rated load to very light load. In the proposed control, duty cycle modulation, switching frequency modulation, and phase shift modulation between active bridges are simultaneously varied in order to maintain constant dc voltage. The two control variables viz., switching frequency and duty ratio are simultaneously adjusted keeping phase shift fixed, in order to regulate voltage with respect to load variations and increase in the input voltage. Whereas, the third control variable, i.e., phase shift regulates output voltage when input from renewable sources is reduced, by keeping frequency and duty ratio fixed. The three control variables provide the greater degree of freedom. The experimental and simulation results of the programmable triplen control are presented for a resonant converter operating from the rated load of 3 kW to 5% of rated load 0.15 kW. The proposed control also tested for the input voltage range of 180–260 V (i.e., 220 V, ± 18% tolerance) in order to validate the functionality of the proposed control.

INDEX TERMS Switching frequency, DC-DC converter with active bridges, phase shift control, duty cycle, zero voltage switching (ZVS).

I. INTRODUCTION

Globally, electrical energy consumption is rising day-by-day consequently imposes the condition to produce increased power efficiently. With ever-increasing concerns on energy crisis, the researchers are more inclined towards development of renewable energy resources (RERs). The review of literature presented here is organized sequentially in the areas of RERs, Power electronics and control using dual active bridge (DAB) converter.

The review of wind power, photovoltaic (PV) and their maximum-power-point tracking (MPPT) to efficiently harness the available renewable energy was reported in [1]–[3]. The above systems have higher reliability, lower complexity, cost and lesser mechanical stress on wind generators. Similarly, an overview of the structures for the distributed power generation systems (DPGS) based on fuel cell, PV, wind power connected to the utility network was presented in [4]. The above structures met with latest set standards regarding power quality, safe running and islanding protection.

In the present day power-system scenario, where the intermittent energy source constitutes an integral part, power electronics plays a vital role for better energy yield. A review of new trends in power converters used for the integration of RERs with/without storage-system technology was presented in [2]. The review was based on reliability and maturity in technology. The other aspect is that RERs produce low output voltage. Hence in a sustainable energy system the use of high gain DC-DC converters become essential to build up the voltage. A significant limitation of conventional DC-DC boost converters required a high duty ratio to provide enhanced gain. Further, it resulted in problems like electromagnetic interference (EMI), reverse-recovery, low efficiency [5].

The DC-DC Resonant converters were popularly employed to resort upon above technical hitches. Those converters had soft switching, high switching frequency capability

with reduced components size for desired voltage gain. The comparison of various control techniques for resonant converters was discussed in [6]–[12]. Most of the control approaches were based on switching frequency, duty cycle, phase shift and variable inductor control etc. But each control has its own limitation and complexity.

In the past two decades, the extensive work was reported by the researchers in the area of converter control to reduce switching/conduction losses; improved efficiency, voltage regulation under varying load conditions [5]. The research included remarkable contributions such as [13]–[15]. In [13] proposed a new transformer-less inverter structure to increase efficiency by eliminating leakage currents, with the aid of 'Lyapunov Stability Theorem'. In [14] presented an observer-based control scheme to estimate input voltage and resistive load. The control scheme showed outstanding performance. The various measures to overcome the limitations of earlier methods through a new two-stage DC–AC symmetric multi-level inverter with modified Model Predictive Control (MMPC) for (PV) applications are discussed in [15].

The prominent attribute of all the above approaches was their applicability for unidirectional power flow control. However, due to inherent variable nature of RERs, there exists a mismatch between generation and load. In order to overcome this mismatch, energy storage is an imperative need of the system. The system demands for a bidirectional power flow interface between the storage system and the local grid. Wherein storage system acts as energy reservoir and maintains the balance between demand and supply. The dual active bridge (DAB) had soft-switching, step-up and step- down operation, simple structure, highly efficient and bidirectional power flow competency [16]. Hence the dual active bridge converters became the best suitable proposition to address the above issues. For a traditional DAB converter with phase-shift modulation [17], the ZVS range was limited by the voltage conversion ratio and load conditions [18]. Reference [19] introduced duty-cycle modulation in one side of a DAB converter to extend the ZVS range and reduce the transformer RMS current.

Optimal phase-shift pairs derived with extended DPS control were further proposed by [20] to minimize reactive power losses. In [21] and [22], advanced modulation methods such as trapezoidal modulation (TZM) and triangular modulation(TRM) had been presented, where the transformer current was modulated in triangular or trapezoidal waveforms to reduce the conduction and the switching loss. References [23]–[25] attempted a hybrid modulation strategy. The strategy was the combination of various existing modulation schemes. The results depicted significant improvement in the efficiency over a wide operating range. In [26] researchers had assorted two different phase-shift modulation to achieve improved transient response accompanied by minimum transient time.

However, all the above methods for DAB converters seems to deal with improved converter performance either over a wide range of input voltage or centering on the enhanced enactment under varying loads. However, there is dearth of studies focusing on objective function of the voltage regulation with respect to varying input voltage and load simultaneously.

Hence, there is an acute need to develop a controller which justifies its suitability for the environment where both load and input voltage variations are prevalent. The proposed controller is a combination of three control variables *viz.* switching frequency, duty ratio and phase shift between two active bridges to regulate output voltage in a DC micro grid with respect to load as well as input voltage variations.

The two-port Modified series parallel resonant converter is presented with the following attributes:

1) The converter gives satisfactory performance when supplied voltage from renewable energy sources is varied from 180V-260V (i.e. 220V, $\pm$ 18% tolerance) and also from a full load of 3kW to 5% of full load i.e. 0.15kW.

2) The control technique provides high conversion efficiency due to soft-switching of all the switches.

3) It is a centralized control of voltage regulation by using digital signal processor (DSP) with switching frequency, duty ratio as well as phase shift between the square wave voltages as control variables.

4) The control approach is decoupled i.e. each control parameter can be adjusted independently.

5) The symmetrical duty cycle of all the switches eliminates the possibility of HF transformer saturation.

The converter with proposed control is shown in Fig. 1(a) analyzed under steady state as presented in the following sections. A control technique for load voltage regulation with respect to load as well as with input voltage variations is discussed in Section 2, along with a mathematical modeling. Simulations and experimental results are presented in Section 3. The conclusion of the paper is presented in section 4.

II. MATHEMATICAL MODELING OF TRIPLEN CONTROL

The control approach for DC output voltage regulation with respect to load and with respect to changing input voltage is designed using three control variables f_s, d, and ϕ_{12}. The phase shift, ϕ_{12} is the phase difference between the square wave voltages of the input and output active bridges. Two control variables f_s and d are used to regulate output with respect to load, keeping phase shift constant. The control variable ϕ_{12} is used to regulate output voltage with respect to input voltage, keeping switching frequency and duty cycle fixed. The phase shift, ϕ_{12} is considered positive if v_{AB} leads $v_{A'B'}$ and power flows from source to load.

In the conventional switching frequency control, switching frequency is varied to control output voltage. Whereas, in duty cycle control, output voltage is maintained by changing duty ratio. The resonant frequency ω_0 of the Modified series parallel resonant tank circuit shown in fig. 1(b), can be expressed using (1) as discussed in [30] and [31]. The circuit model of this tank is as shown in fig. 1(c).

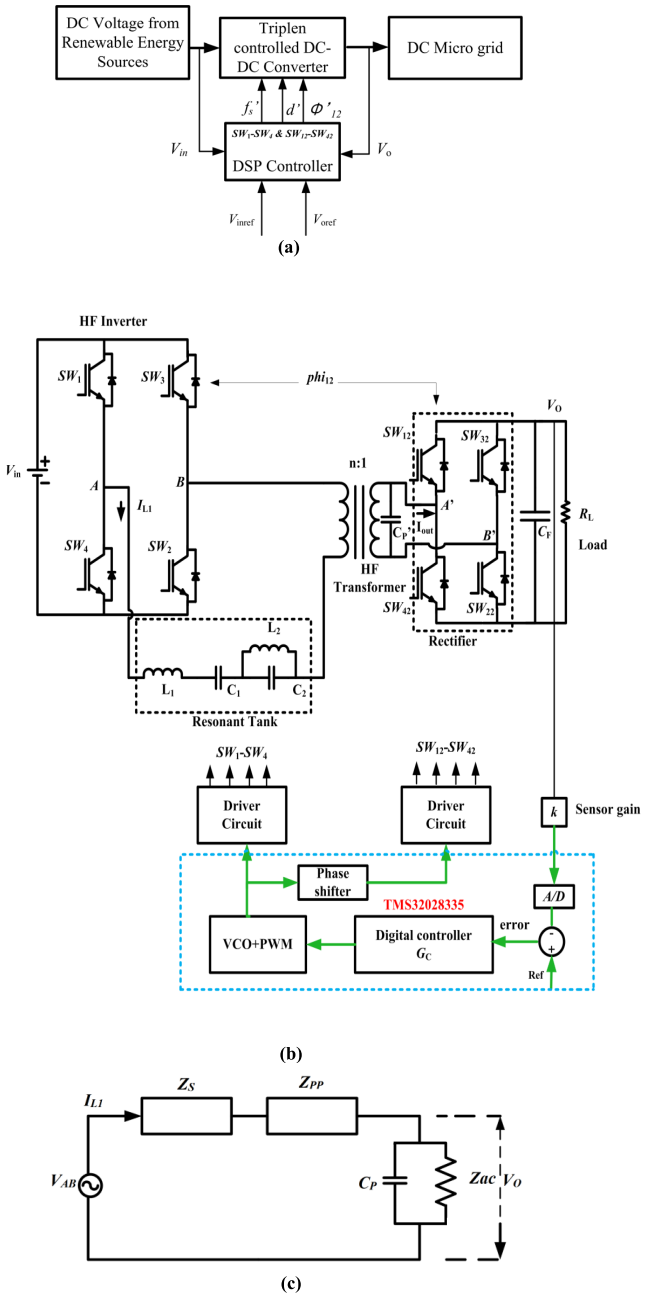

FIGURE 1. (a) Proposed triplen controller, (b) Full active bridge higher order resonant tank, (c): circuit model of full active bridge tank.

The proposed controller exhibits control during two distinct conditions: (i) when load is reduced and (ii) when input voltage from renewable source is varying. Because of the controlled rectifier on output port, the rectifier output voltage and current are not always in phase. Thus, it is valid to represent the whole secondary part of the circuit with equivalent impedance Z_{ac} instead of a pure resistance, R_{ac} using (2) [27].

$$\omega_0 = \sqrt{[(\frac{1}{2L_1C_1})\alpha(\beta + \sqrt{\beta^2 - 4})]} \tag{1}$$

where, $\alpha = \sqrt{\frac{C_1}{C_2}\frac{L_1}{L_2}}$ and

$$\beta = \sqrt{\frac{C_1}{C_2}\frac{L_1}{L_2}} + \sqrt{\frac{C_1}{C_2}\frac{L_2}{L_1}} + \sqrt{\frac{C_2}{C_1}\frac{L_2}{L_1}}$$

$$Z_{ac} = \frac{8R'_L \cos\gamma}{\pi^2} = R_{ac}\cos\gamma \tag{2}$$

where,

$$\gamma = \phi - \phi_{12}$$

$$Z_p = \frac{-jZ_{ac}}{(\omega_s C_p Z_{ac} - j)} \tag{3}$$

$$Z_s = (j\omega_s L_1 - \frac{j}{\omega_s C_1}) \tag{4}$$

$$Z_{pp} = \frac{-j\omega_s L_2}{(\omega_s^2 C_2 L_2 - 1)} \tag{5}$$

$$Z_{in} = Z_p + Z_s + Z_{pp} \tag{6}$$

The total impedance of the resonant tank Z_{in} is function of switching frequency ω_s, as expressed in (6). The phase angle of impedance Z_{in} is also the function of switching frequency ω_s and expressed using (7).

$$\phi = g(\omega_s) = \tan^{-1}[\frac{\omega_s L_1 - \frac{1}{\omega_s C_1} - \frac{\omega_s L_2}{\omega_s^2 L_2 C_2 - 1} - \frac{\omega_s C_p Z_{ac}^2}{1+\omega_s^2 C_p^2 Z_{ac}^2}}{\frac{Z_{ac}}{1+\omega_s^2 C_p^2 Z_{ac}^2}}] \tag{7}$$

A. WHEN LOAD IS REDUCED

On light loads as well as during high input voltage, output terminal voltage tends to increase and hence decrease in voltage gain is required to regulate output voltage. During this condition, the proposed controller simultaneously adjusts duty ratio and frequency both, keeping phase shift fixed in order to maintain desired output voltage. This will regulate the output voltage with lesser variation in frequency and duty cycle due to two control variables. The steady state performance is analyzed assuming sinusoidal resonant currents and voltages. If duty ratio for all the switches is d, then input voltage applied to resonant tank network, $v_{AB}(t)$ that circulates current $i_L(t)$ in the tank circuit can be estimated using (8) [33], [34].

$$v_{ABac}(t) = 2\sqrt{2}\frac{V_{in}}{\pi}[1 - \cos(2\pi d)]^{1/2}\sin(\omega t + \psi) \tag{8}$$

The phase angle of voltage $v_{AB}(t)$, ψ is a function of duty ratio d and can be expressed using (9). Equation (10) determines the overall converter voltage gain in terms of frequency and duty cycle [28].

$$\psi = f(d) = \tan^{-1}[\frac{\sin(2\pi d)}{1 - \cos(2\pi d)}] \tag{9}$$

$$M = \frac{V_0}{V_{in}} = \frac{2Z_p}{n\pi Z_{in}}\sqrt{1 - \cos 2\pi d} = K_1\frac{Z_p}{Z_{in}}\sin(\pi d) \tag{10}$$

where,

$$K_1 = \frac{2\sqrt{2}}{n\pi}$$

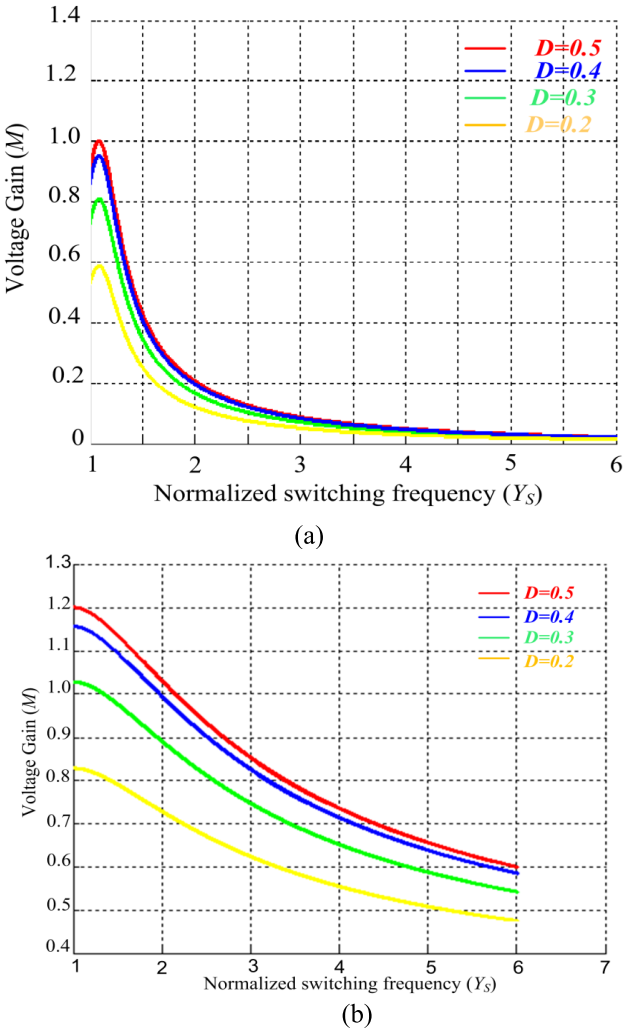

FIGURE 2. Variation of gain with switching frequency as a function of duty ratio at: (a) rated, (b) 30% rated load.

The variation of converter voltage gain, M with normalized switching frequency, Y_S at different duty cycles for full load and for 30% rated load are shown in Fig. 2(a)-(b). The effect of variations of duty cycle is more effective at lighter load rather than full load [28].

Using the developed algorithm, renewed switching frequency, f_S' and renewed duty cycle d' are computed corresponding to change in the output voltage due to changing loads using (12)-(13). If V_O and V_{Oref} are actual output voltage and reference output voltage respectively, then the actuating control voltage, v_C can be calculated using (11), The k′ is proportionality constant to step down voltage.

$$v_C = k'\left(V_o - V_{Oref}\right) \tag{11}$$
$$f_S' = f_S + v_C k_f \tag{12}$$
$$d' = d - v_c k_d \tag{13}$$

The instantaneous value of resonant current, i_{L1} flowing through the resonant network can be calculated

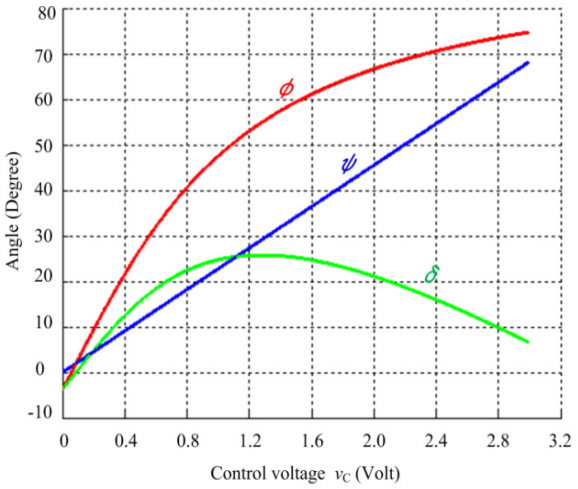

FIGURE 3. Variation in various angles with v_C.

using (14)

$$i_{L1}(t) = \frac{2\sqrt{2}V_{in}}{\pi Z_{in}}[1 - \cos 2\pi d]^{1/2}\sin(\omega t + \psi - \phi) \tag{14}$$

For ZVS operation, the resonant inductor current i_{L1}(t) must lag the square wave voltage v_{AB}(t) and angle δ must be positive.

$$\delta = \phi - \psi > 0$$
$$\phi > \psi \tag{15}$$

The various angles $\delta = h(\omega_s, d)$, $\phi = g(\omega_s)$ and $\psi = f(d)$ are plotted against control voltage, v_C and depicted in Fig.3. The angle δ is greater than zero over a wide range during proposed approach. Therefore, ZVS is ensured if renewed frequency, f_S' and renewed duty cycle d' are kept within limits.

B. WHEN INPUT VOLTAGE FROM RENEWABLE SOURCES REDUCED

When input voltage is reduced and converter is on full load then converter output voltage tends to be reduced. Therefore, increase in converter gain is required to get required output DC bus voltage.

1) NECESSITY OF THIRD CONTROL VARIABLE

It is very important to note that, if increase in gain is required, duty ratio d should be increased which is not possible as it has already been set to maximum at full load. The gain can be increased by reducing switching frequency ω_s which is also not possible as it has already been set to resonant frequency at full load. The switching frequency cannot be reduced below the resonant frequency otherwise soft switching may be lost. Therefore, under this condition, third control variable ϕ_{12} is necessary to regulate output voltage with respect to decrease in input voltage from renewable energy sources. The angle ϕ_{12} is the shift in phase between the square wave voltages of input and output ports. The phase shift, ϕ_{12} is considered positive if $v_{A'B'}$ lags v_{AB}. It is stated that the voltage gain

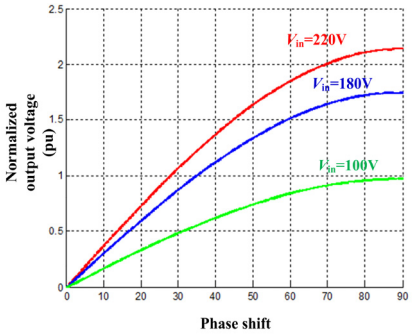

FIGURE 4. Variation of normalized output voltage with phase shift for diff. input voltages.

of a two active port converter with load side active bridge is greater than that with load side diode rectifier bridge [29]. The phase shift between two ports of converter can be varied from 0° to 90°. If the load resistance is R_L, transformer turns ratio is n and load current is I_o, then output voltage $V_o = I_o R_L$ can be expressed in terms of phase shift, ϕ_{12} by using (16),

$$M_2 = \frac{n}{m}\sin(\phi_{12}) \tag{16}$$

$$m = Q\left(Y_s - \frac{1}{Y_s}\right) \tag{17}$$

$$Y_s = \frac{\omega_s}{\omega_o} \tag{18}$$

$$Q = \frac{\omega_0 L_1}{R'_L} \tag{19}$$

The angle of phase shift, ϕ_{12} is set to be positive to have power flow from port 1 to port 2. Fig. 4 shows that converter gain and hence output voltage increases with increase in phase shift between active bridges.

2) CONDITION FOR ZVS DURING TRIPLEN CONTROL

The condition for soft switching in the active bridges states that, if port 1 current, i_{L1} lags its applied square wave voltage, v_{AB} then all switches in port 1 bridge operate at zero-voltage switching. However for bridge 2, the condition for ZVS states that, if port 2 current, i_{out} leads its applied square wave voltage, $v_{A'B'}$ then all switches in port 2 bridge operate at zero-voltage switching. These conditions are checked and satisfied by the proposed triplen control technique.

The proposed algorithm estimates suitable renewed phase shift, ϕ'_{12}, according to change in the input voltage from renewable source using (20). If v_{in} and v_{inref} are actual input voltage and input voltage reference respectively, then actuating control voltage, v could be calculated using (21), with k_1 as a scaling factor to step down voltage to the level tolerated by DSP. k_p is a phase shift constant.

$$\phi'_{12} = \phi_{12} + kp * v \tag{20}$$

$$v = k_1(v_{inref} - v_{in}) \tag{21}$$

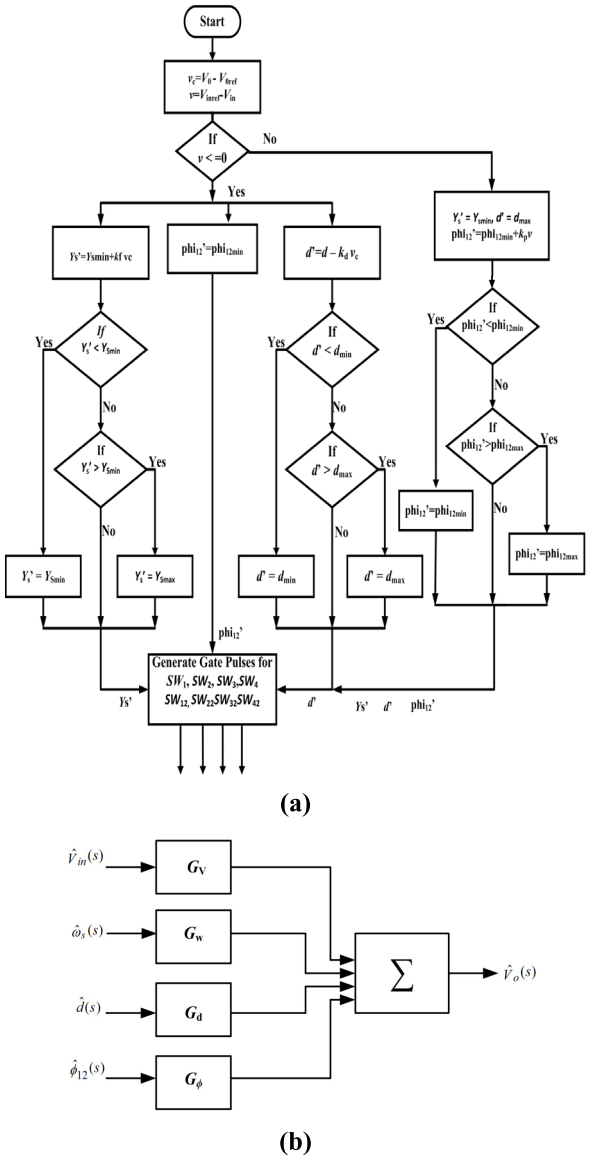

FIGURE 5. (a) Proposed control algorithm, (b) Mathematical representation of small signal model of the converter.

Fig. 5(a), shows the control flow of proposed algorithm. It estimates appropriate switching frequency, duty ratio and phase shift for regulating output voltage with respect to load and input voltage variations. The control algorithm is implemented using digital controller DSP TMS320F28335. The normalized switching frequency has a lower limit of Y_{Smin} which is slightly greater than normalized resonant frequency Y_{So} to avoid operation below resonant frequency. The range of normalized switching frequency is kept between $Y_{Smin} = 1.06$ and $Y_{Smax} = 1.90$, duty ratio to be $d_{min} = 0.16$ to $d_{max} = 0.48$ and phase shift, $\phi_{12\min} = 5°$ to $\phi_{12max} = 90°$ for ZVS operation of the switches. When input voltage is reduced, the coarse tuning is achieved by phase shift control and fine tuning by switching frequency and duty ratio.

In the proposed controller, a suitable control scheme is very essential for good voltage regulation and soft switching operation. It can be observed from (10) and (16) that dc output grid voltage V_0 is regulated using switching frequency f_s, duty ratio d and on external phase shift ϕ_{12} as control variables. Therefore, output voltage can be regulated by varying f_s, d with respect to changes in DC load and by varying ϕ_{12} with respect to changes in input voltage. A closed loop control scheme for the proposed converter is shown in Fig. 1(b). An error signal is generated by comparing the output voltage V_0 with the reference signal. The error signal is processed through a compensator i.e. digital controller and it sends an actuating signal to a modulator. The modulator will generate a switching pattern with desired switching frequency, duty ratio and external phase shift, which is then sent to the driver circuitry. Design of compensator Gc and voltage control oscillator is presented in the following.

a: COMPENSATOR DESIGN

Fig. 5(b) shows the mathematical representation of the converter's small signal model. The $\hat{V}_{in}(s)$, $\hat{\omega}_s(s)$, $\hat{d}(s)$ and $\hat{\phi}_{12}(s)$ are the Laplace transform of small perturbations in $\hat{V}_{in}(t)$, $\hat{\omega}_s(t)$, $\hat{d}(t)$ and $\hat{\phi}_{12}(t)$ respectively. The $\hat{V}_{in}(t)$, $\hat{\omega}_s(t)$, $\hat{d}(t)$ and $\hat{\phi}_{12}(t)$ are the perturbations in $V_{\text{in}}(t)$, $d(t)$, $\omega_s(t)$ and $\phi_{12}(t)$ of the converter system respectively. As stated by the law of superposition, the resultant output voltage perturbation is the sum of individual control to output perturbations when other control inputs are set to zero. Therefore, the total dc grid voltage perturbation can be given as;

$$\hat{V}_o(s) = G_v.\hat{V}_{in}(s) + G_\omega.\hat{\omega}_s(s) + G_d.\hat{d}(s) + G_\phi.\hat{\varphi}_{12}(s) \quad (22)$$

If $\hat{V}_{in}(s)$ equal to zero in (22), as it is not the control variable perturbation, the dc grid voltage perturbation $\hat{V}_o(s)$can be determined in terms of switching frequency, duty ratio and phase shift perturbations as follows;

$$\hat{V}_o(s) = G_\omega.\hat{\omega}_s(s) + G_d.\hat{d}(s) + G_\phi.\hat{\varphi}_{12}(s) \quad (23)$$

where, G_V is the open-loop control ($\hat{V}_{in}(s)$) to output ($\hat{V}_o(s)$) transfer function, G_d is the open-loop control ($\hat{d}(s)$) to output ($\hat{V}_o(s)$) transfer function, G_ω is the open loop control ($\hat{\omega}_s(s)$) to output ($\hat{V}_o(s)$) transfer function and G_ϕ is the open loop control ($\hat{\varphi}_{12}(s)$) to output ($\hat{V}_o(s)$) transfer function in a small signal model as shown in Fig. 5(b). The derivation of open-loop control to output transfer functions in a small-signal model and the corresponding compensator design based on loop shaping are discussed in [30]. Implementation of the voltage control loop in power electronics applications, digital controller is a viable option as they are more robust and can be simply manipulated for optimal control performance when compared to analog controllers. In this paper, the voltage control loop algorithm can be implemented using TMS32028335 control card, which is a 32-bit floating point digital signal processor (DSP) microcontroller. Fig. 5(a) shows flow chart that could be used to implement the voltage control loop for dc/dc converter. The voltage control oscillator (VCO) is used to produce variable frequency, variable duty ratio pulses based on the control voltage which is realized with a digital signal processor.

TABLE 1. Specifications of the converter.

Voltage input range	260V-180V
Specified Voltage input	220V
Specified Output Voltage	400V
P_O	3000W
Resonant frequency	100kHz
Series tank parameters	L_1=51.35µH , C_1 = 54.32nF
Parallel tank parameters	L_2 = 513.5µH , C_2= 543.2nF
Parallel capacitor	C_P=5.432nF, C_P'=n^2C_P =1.643nF
Capacitor filter	0.2 nF
Ultra-fast switches, IGBTs	30N60A4D
HF Transformer	Ferrite core PM 62, n = 0.55

TABLE 2. Performance of prototype under Triple hybrid control ($\phi_{12} = 20°$).

Parameters	FL	3/4th FL	1/2th FL	1/10th FL	1/20th FL
$R_L(\Omega)$	**54**	**72**	**107**	**540**	**1067**
Freq. control	106	112	250	333.5	398
Duty ratio control (d)	0.48	0.46	0.43	0.26	0.16
Triplen control (f_s, d')	f_S'=106 , d'=0.48	f_S'=108 , d'=0.48	f_S'=111, d'=0.47	f_S'= 148 , d'=0.32	f_S'=170 , d'=0.27

III. EXPERIMENTAL AND SIMULATION RESULTS

A. SIMULATION RESULTS

The triplen control technique is tested using PSIM simulation for a 3 kW, 220/400V Modified series parallel resonant converter prototype with a switching frequency of 106 kHz. The converter parameters are as shown in Table 1.

The simulation results of converter during load variation with variable frequency and duty cycle with fixed phase shift are shown in Table 2. It reveals that the voltage regulation is achieved with 170 kHz frequency and $d = 0.27$ at 5% rated load whereas it was 398 kHz during conventional switching frequency control and $d = 0.16$ during conventional switching duty ratio control. This frequency reduction drastically reduces the switching loss and reduction in duty cycle results in reduced conduction loss, and hence improves the conversion efficiency dramatically.

B. EXPERIMENTAL RESULTS

To check the functionality of the proposed control the converter is experimentally tested under variable load and variable input voltages. The dynamic performance is evaluated

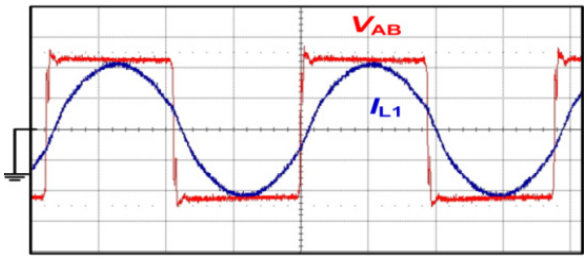

FIGURE 6. Applied port 1voltage v_{AB} and tank current at rated load. (100V/ division, 10A/ division).

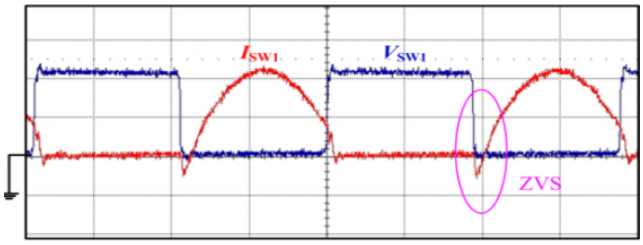

FIGURE 7. Switch voltage and current at rated load (100V/ division, 10A/ division).

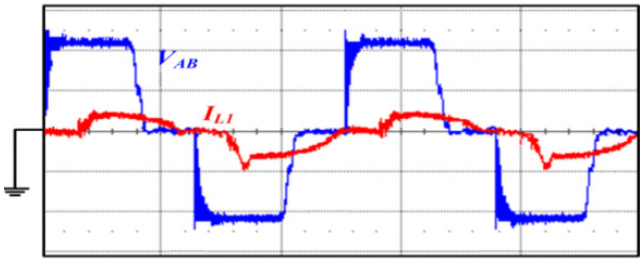

FIGURE 8. Applied port 1voltage v_{AB} and resonant tank current at 5% rated load (100V/division, 5A/division, 2.5μs/division).

with step changes in supply voltage and presented in the following section.

1) WHEN LOAD IS REDUCED

During this operation, phase shift, Φ_{12} is kept constant at 20°. Fig.6-Fig.8, illustrate the important experimental waveforms when converter was operated from rated load to 5% rated load. Fig. 6 shows the square wave voltage input of the resonant tank of port 1, v_{AB} and resonant inductor current, i_{L1} during rated load power of 3kW, when operating at 106 kHz and $d = 0.48$. The current, i_{L1} is lagging voltage, v_{AB} which ensures ZVS of all the switches of port1. Fig. 7 shows the voltage and current of switch SW_1 of port1 which reveals soft switching operation. Fig.8 illustrates the voltage input to the resonant tank, v_{AB} and tank current, i_{L1} at 5% rated load; when operating at 161 kHz and $d = 0.27$.

2) WHEN INPUT VOLTAGE IS REDUCED

In this operation, the load is at its rated value of 3kW, switching frequency is $f_s = f_{smin} = 106$ kHz. and $d = d_{max} = 0.48$.

TABLE 3. (a) Variation of phase shift w.r.t. reduction in input voltage at rated load ($f_s = 106$kHz, $d = 0.499$). (b) Variation of control variables w.r.t. increase in input voltage at rated load ($\Phi_{12} = 20°$).

(a)

V_{in} (V)	Φ_{12}(deg.)	I_{L1}(A, peak)	I_{out}(A, peak)	*Efficiency (%)*
220	20	21.46	11.7	98.37%
200	25	23.91	13.03	95 %
180	32	29.86	16.27	92.23%

(b)

V_{in} (V)	f_s (kHZ), d'	I_{in} (A)	I_{L1}(A, peak)	I_{out}(A, peak)	*Efficiency (%)*
220	f_s=106, d=0.48	14.07	21.59	11.77	98.37
230	f_s=107, d=0.48	13.48	20.61	11.23	96.76
242	f_s=106, d=0.43	12.61	21.08	11.49	98.3
260	f_s=110.5, d=0.43	12.37	21.25	11.58	93.27

The frequency is at its minimum value and duty cycle is at its maximum value. The main concern of the proposed triplen control is the converter performance under reduced input voltage at rated load. The input voltage is gradually reduced from its specified value i.e. from $V_{in} = 220$ V. It is observed that DC output voltage is regulated at 400V when input voltage is reduced with the consequent increase in phase shift. Different input voltages and corresponding phase shifts are illustrated in Table 3. It could be seen that by increasing phase shift from 10° to 32°, output DC voltage is regulated when input voltage from renewable source was reduced from 260 V to 180 V.

When the converter is tested at $V_{in} = 200$V and $V_{in} = 180$V with load at its rated value 3kW. The control algorithm at this condition operates at initial operating point ($f_s = 106$ kHz, d=0.499, $\phi_{12} = 20°$). Fig.9-16 show the key experimental waveforms when converter at $V_{in} = 200$V and 180V. All the pulses during phase shift control are at 50%. Fig. 9 illustrates that the tank current I_{L1} lags its applied voltages, $v_{AB}(t)$. Fig. 10 shows that the port 2 current I_{out} leads the voltage, $v_{A'B'}(t)$ at $V_{in} = 200$ V and hence, ZVS occurs in all the switches of port1 and port2. The two square wave voltages at primary and secondary side bridges are at $\phi_{12} = 25°$ as shown in Fig. 11. The fig. 12 shows output voltage, input voltage and load current at $V_{in} = 200$ V. Hence, DC voltage is regulated at 400V when supply voltage is reduced to 200V, with an operating point ($f_s = 106$ kHz, d=0.499, $\phi_{12} = 25°$).

Similarly, all the operational waveforms during the experimentation at $V_{in} = 180$ V are shown in Fig. 13-16. Fig. 13-14 show that port 1 tank current lags port 1 voltage v_{AB} and port 2 tank current leads port 2 voltage $v'_{A'B}$

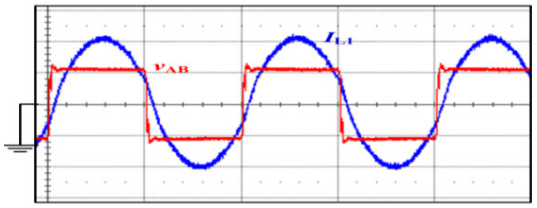

FIGURE 9. Applied port 1voltage v_{AB} and port 1 tank current at rated load at V_{in} = 200V. (200V/division, 10A/ division, 5μs/ division).

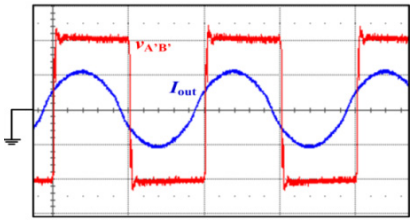

FIGURE 10. Applied port 2 voltage $v_{A'B'}$ and port 2 current at rated load with V_{in} = 200V (200V/ division, 10A/ division, 5μs/ division).

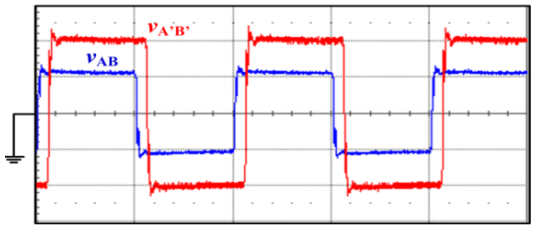

FIGURE 11. Applied port 1 voltage v_{AB} and applied port 2 voltage $v_{A'B'}$ at rated load with V_{in} = 200V (200V/ division, 10A/division, 5μs/ division).

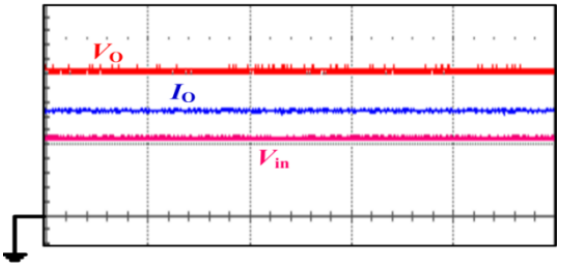

FIGURE 12. Port 2 output voltage V_O and port 1 applied voltage V_{in} and output dc current at rated load (200V/ division, 10A/ division, 5μs/ division).

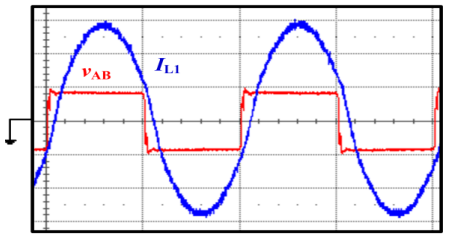

FIGURE 13. Applied port 1voltage v_{AB} and port 1 tank current at rated load at V_{in} = 180V. (200V/ division, 10A/ division, 5μs/ division).

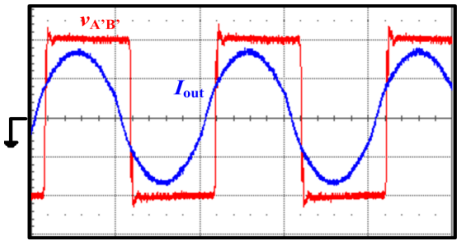

FIGURE 14. Applied port 2 voltage $v_{A'B'}$ and port 2 current at rated load at V_{in} = 180V. (200V/ division, 10A/ division, 5μs/ division).

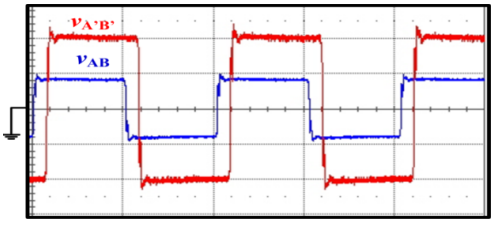

FIGURE 15. Applied port 1 voltage v_{AB} and applied port 2 voltage $v_{A'B'}$ at rated load with V_{in} = 180V. (200V/ division, 10A/ division, 5μs/ division).

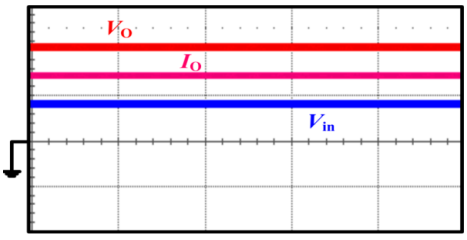

FIGURE 16. Port 2 output voltage V_O and port 1 applied voltage V_{in} and output dc current at rated load (200V/ division, 10A/ division, 5μs/ division).

respectively at V_{in} = 180 V. It means all the switches of port 1 and port 2 are operating at ZVS. Fig. 16 shows that output voltage is maintained at 400 V during the reduced input of V_{in} = 180 V with an operating point (f_s = 106 kHz, d=0.499, $\phi_{12} = 32°$).

To study the dynamic performance using triplen control, input voltage is changed in step from specified value of V_{in} = 220 V. Firstly, the converter input is reduced from 220 V to 200 V at instant $t_1 = 0$. The comparison of dynamic response for step change in input voltage using conventional frequency control and proposed control is shown in Fig.17. It depicts that with triplen control, the settling time is reduced to $\Delta x_2 = 0.05$ ms and response peak is reduced to 394 V i.e. percentage undershoot $\%\Delta v_2 = 1.5\%$ whereas, settling time was $\Delta x_1 = 0.1$ ms and response peak was 390 V i.e. $\%\Delta v_1 = 2.5\%$ with conventional frequency control.

Similarly, when the converter input is increased from 220 V to 260 V at instant $t = 0$. The comparison of dynamic responses using classical frequency control and triplen control is shown in Fig.18. It shows that the settling time was $\Delta t_1 = 0.05$ms and response peak is 405 V

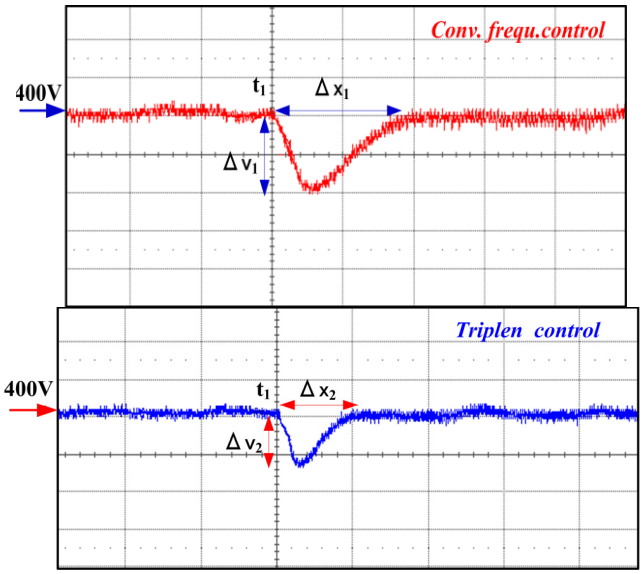

FIGURE 17. Dynamic performance using frequency control and triplen control due to step change of input from 220 V to 200; (voltage scale: 5 V/division, time scale: 0.05 *ms/div.*).

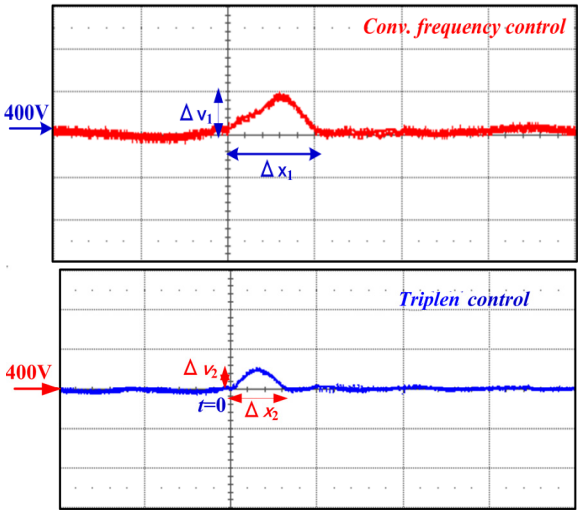

FIGURE 18. Dynamic performance using frequency control and triplen control due to step change of input from 220 V to 260 V; (voltage scale: 5 V/division, time scale: 0.05 ms/div.).

i.e. percentage peak overshoot,$\%M_{P1} = 1.25\%$ with conventional frequency control. However, with triplen controller the settling time is reduced to $\Delta t_2 = 0.03$ ms and response peak is 401 V i.e. percentage overshoot, $\%M_{P2} = 0.62\%$. It is seen that settling time and peak overshoot are reduced considerably, which implies significant improvement in the dynamic performance when proposed controller is used.

Table 4 shows the comparison of efficiencies achieved with proposed control and those during conventional controls. The proposed triplen gives high efficiencies with respect to varying loads as well as input variations.

TABLE 4. Comparison of the efficiency with classical control techniques.

Load	Conv. frequency control	Conv. duty ratio control	Proposed Triplen Control V_{in}=220V
FL	97.6 %	97.6 %	98.37%
75% FL	97 %	96.5%	98.2 %
50% FL	96.1%	95.78%	97.54 %
10% FL	82.94 %	92.2%	91.51 %
5% FL	73.47 %	80%	86.7 %

IV. CONCLUSION

In this paper, triplen controller using three control variables for modified series parallel resonant tank converter is proposed to interface renewable sources to DC bus in a micro grid. This controller provides excellent performance in terms of ZVS, improved efficiency, voltage regulation with respect to reduced input voltage from renewable sources at full load. The analysis and experimental results show that the proposed triplen controller has a capability to provide voltage regulation in the environment where both load and input voltage variations are prevalent. In this controller switching frequency and duty ratio are simultaneously varied for voltage regulation with respect to load. The proposed control can also regulate constant DC bus voltage by changing phase shift between two active bridges when input voltage from renewable sources is reduced. It is observed from the figures (9)-(10) & (13)-(14) illustrate that the tank current lags behind its applied voltage in port 1 and port 2 current leads its applied voltage in port 2. Therefore, ZVS occurs in all the switches of port 1 as well as of port 2. Three control variables provide advantages such as more degree of freedom and less frequency excursions. Experimental results verify the functionality of proposed controller.

REFERENCES

[1] K. T. Chau, Y. S. Wong, and C. C. Chan, "An overview of energy sources for electric vehicles," *Energy Convers. Manage.*, vol. 40, no. 10, pp. 1021–1039, 1999.

[2] J. M. Carrasco *et al.*, "Power-electronic systems for the grid integration of renewable energy sources: A survey," *IEEE Trans. Ind. Electron.*, vol. 53, no. 4, pp. 1002–1016, Jun. 2006.

[3] J.-H. Teng, W.-H. Huang, T.-A. Hsu, and C.-Y. Wang, "Novel and fast maximum power point tracking for photovoltaic generation," *IEEE Trans. Ind. Electron.*, vol. 63, no. vol. 8, pp. 4955–4966, Apr. 2016.

[4] F. Blaabjerg, R. Teodorescu, M. Liserre, and A. V. Timbus, "Overview of control and grid synchronization for distributed power generation systems," *IEEE Trans. Ind. Electron.*, vol. 53, no. 5, pp. 1398–1409, Oct. 2006.

[5] Y.-P. Hsieh, J.-F. Chen, T.-J. P. Liang, and L.-S. Yang, "Novel high step-up DC–DC converter with coupled-inductor and switched-capacitor techniques for a sustainable energy system," *IEEE Trans. Power Electron.*, vol. 26, no. 12, pp. 3481–3490, Dec. 2011.

[6] J.-H. Jung and J.-G. Kwon, "Theoretical analysis and optimal design of LLC resonant converter," in *Proc. Eur. Conf. Power Electron. Appl.*, Sep. 2007, pp. 1–10.

[7] J. H. Jung, J.-M. Choi, and J.-G. Kwon, "Design methodology for transformers including integrated and center-tapped structures for LLC resonant converters," *J. Power Electron.*, vol. 9, no. 2, pp. 215–223, Mar. 2009.

[8] S.-Y. Chen, Z. R. Li, and C.-L. Chen, "Analysis and design of single-stage AC/DC *LLC* resonant converter," *IEEE Trans. Ind. Electron.*, vol. 59, no. 3, pp. 1538–1544, Mar. 2012.
[9] X. Fang, H. Hu, Z. J. Shen, and I. Batarseh, "Operation mode analysis and peak gain approximation of the LLC resonant converter," *IEEE Trans. Power Electron.*, vol. 27, no. 4, pp. 1985–1995, Apr. 2012.
[10] J. Zhang, J. Liao, J. Wang, and Z. Qian, "A current-driving synchronous rectifier for an LLC resonant converter with voltage-doubler rectifier structure," *IEEE Trans. Power Electron.*, vol. 27, no. 4, pp. 1894–1904, Apr. 2012.
[11] J.-H. Jung, H.-S. Kim, M.-H. Ryu, and J.-W. Baek, "Design methodology of bidirectional CLLC resonant converter for high-frequency isolation of DC distribution systems," *IEEE Trans. Power Electron.*, vol. 28, no. 4, pp. 1741–1755, Apr. 2013.
[12] M. Z. Youssef and P. K. Jain, "A review and performance evaluation of control techniques in resonant converters," in *Proc. 30th Annu. Conf. IEEE Ind. Electron. Soc. (IECON)* vol. 1, Nov. 2004, pp. 215–221.
[13] T. Jalilzadeh, M. T. Hagh, and M. Sabahi, "Analytical study and simulation of a transformer-less photovoltaic grid-connected inverter with a delta-type tri-direction clamping cell for leakage current elimination," *Compel-Int. J. Comput. Math. Elect. Electron. Eng.*, vol. 37, no. 2, pp. 814–831, 2018.
[14] M. Malekzadeh, A. Khosravi, and M. Tavan, "Observer based control scheme for DC-DC boost converter using sigma–delta modulator," *Compel-Int. J. Comput. Math. Elect. Electron. Eng.*, vol. 37, no. 2, pp. 784–798, 2018.
[15] M. Maalandish, S. H. Hosseini, M. Sabahi, and P. Asgharian, "Modified MPC based grid-connected five-level inverter for photovoltaic applications," *Compel-Int. J. Comput. Math. Elect. Electron. Eng.*, vol. 37, no. 2, pp. 971–985, 2018.
[16] Y. Shi, R. Li, Y. Xue, and H. Li, "Optimized operation of current-fed dual active bridge DC-DC converter for PV applications," *IEEE Trans. Ind. Electron.*, vol. 62, no. 11, pp. 6986–6995, Nov. 2015.
[17] R. W. De Donker, D. M. Divan, and M. H. Kheraluwala, "A three-phase soft-switched high-power-density DC/DC converter for high-power applications," *IEEE Trans. Ind. Appl.*, vol. 27, no. 1, pp. 63–73, Jan./Feb. 1991.
[18] A. K. Jain and R. Ayyanar, "PWM control of dual active bridge: Comprehensive analysis and experimental verification," *IEEE Trans. Power Electron.*, vol. 26, no. 4, pp. 1215–1227, Apr. 2011.
[19] G. G. Oggier, G. O. García, and A. Oliva, "Switching control strategy to minimize dual active bridge converter losses," *IEEE Trans. Power Electron.*, vol. 24, no. 7, pp. 1826–1838, Jul. 2009.
[20] H. Wen, W. Xiao, and X. Su, "Nonactive power loss minimization in a bidirectional isolated DC–DC converter for distributed power systems," *IEEE Trans. Ind. Electron.*, vol. 61, no. 12, pp. 6822–6831, Dec. 2014.
[21] F. Krismer and J. W. Kolar, "Accurate power loss model derivation of a high-current dual active bridge converter for an automotive application," *IEEE Trans. Ind. Electron.*, vol. 57, no. 3, pp. 881–891, Mar. 2010.
[22] F. Krismer and J. W. Kolar, "Closed form solution for minimum conduction loss modulation of DAB converters," *IEEE Trans. Power Electron.*, vol. 27, no. 1, pp. 174–188, Jan. 2012.
[23] F. Krismer, S. Round, and J. W. Kolar, "Performance optimization of a high current dual active bridge with a wide operating voltage range," in *Proc. IEEE Power Electron. Spec. Conf.*, Jun. 2006, pp. 1–7.
[24] H. Zhou and A. M. Khambadkone, "Hybrid modulation for dual-active-bridge bidirectional converter with extended power range for ultracapacitor application," *IEEE Trans. Ind. Appl.*, vol. 45, no. 4, pp. 1434–1442, Jul./Aug. 2009.
[25] X.-F. He, Z. Zhang, Y.-Y. Cai, and Y.-F. Liu, "A variable switching frequency hybrid control for ZVS dual active bridge converters to achieve high efficiency in wide load range," in *Proc. IEEE Appl. Power Electron. Conf.*, Mar. 2014, pp. 1095–1099.
[26] X. Li and Y.-F. Li, "An optimized phase-shift modulation for fast transient response in a dual-active-bridge converter," *IEEE Trans. Power Electron.*, vol. 29, no. 6, pp. 2661–2665, Jun. 2014.
[27] X. Li and A. K. S. Bhat, "Analysis and design of high-frequency isolated dual-bridge series resonant DC/DC converter," *IEEE Trans. Power Electron.*, vol. 25, no. 4, pp. 850–862, Apr. 2010.
[28] H. M. Suryawanshi *et al.*, "Hybrid control of high-efficient resonant converter for renewable energy system," *IEEE Trans. Ind. Informat.*, vol. 14, no. 5, pp. 1835–1845, May 2018.
[29] H. Krishnaswami and N. Mohan, "Three-port series-resonant DC–DC converter to interface renewable energy sources with bidirectional load and energy storage ports," *IEEE Trans. Power Electron.*, vol. 24, no. 10, pp. 2289–2297, Oct. 2009.
[30] H. M. Suryawanshi, K. L. Thakre, S. G. Tarnekar, D. P. Kothari, and A. G. Kothari, "Power factor improvement and closed loop control of an AC-to-DC resonant converter," *IEE Proc.-Electr. Power Appl.*, vol. 149, no. 2, pp. 101–110, Mar. 2002.
[31] H. M. Suryawanshi and S. G. Tarnekar, "Modified LCLC-type series resonant converter with improved performance," *IEE Proc.-Electr. Power Appl.*, vol. 143, no. 5, pp. 354–360, Sep. 1996.
[32] H. M. Suryawanshi and S. G. Tarnekar, "Improvement of power factor using modified series-parallel resonant converter," in *Proc. IEEE Conf. Power Qual.*, Jun. 1998, pp. 103–109.
[33] Z. Ye, P. K. Jain, and P. C. Sen, "A two-stage resonant inverter with control of the phase angle and magnitude of the output voltage," *IEEE Trans. Ind. Electron.*, vol. 54, no. 5, pp. 2797–2812, Oct. 2007.
[34] J. M. Burdio, L. A. Barragan, F. Monterde, D. Navarro, and J. Acero, "Asymmetrical voltage-cancellation control for full-bridge series resonant inverters," *IEEE Trans. Power Electron.*, vol. 19, no. 2, pp. 461–469, Mar. 2004.

SNEHAL PACHPOR received the B.E. degree in electrical engineering from the Government College of Engineering, Amravati, India, in 1991, and the M.Tech. degree in integrated power systems from the Visvesvaraya National Institute of Technology, Nagpur, India, in 2007, where she is currently pursuing the Ph.D. degree in electrical engineering. She is currently an Associate Professor with the Department of Electrical Engineering, KITS, Ramtek, India. Her current research interests include power electronics, resonant converters, and power quality.

HIRALAL MURLIDHAR SURYAWANSHI (M'06–SM'12) received the B.E. degree in electrical engineering from the Walchand College of Engineering, Sangli, India, in 1988, and the M.E. degree in electrical engineering from the Indian Institute of Science, Bengaluru, India, in 1994, and the Ph.D. degree from Nagpur University, Nagpur, India, in 1999. He is currently a Professor with the Department of Electrical Engineering, Visvesvaraya National Institute of Technology, Nagpur. He is the Chair Professor of INAE. His current research interest includes power electronics, emphasizing developmental work in the area of resonant converters, power factor correction, active power filters, FACTs devices, multilevel converters, and electric drives. He received the Fellow of Indian National Academy of Engineering Award, in 2012, for his outstanding research. He has also received the IETE-Bimal Bose Award, in 2009, and the IETE-Biman Behari Sen Memorial Award, in 2017, for his leadership in Power Electronics in India. He is an Associate Editor of the IEEE TRANSACTIONS ON INDUSTRIAL ELECTRONICS.